SCIENTIFIC REPORTS
natureresearch

Check for updates

OPEN

Demonstration of a pseudo-magnetization based simultaneous write and read operation in a $Co_{60}Fe_{20}B_{20}/Pb(Mg_{1/3}Nb_{2/3})_{0.7}Ti_{0.3}O_3$ heterostructure

Tingting Shen[1,3,4]✉, Vaibhav Ostwal[2,3,4]✉, Kerem Y. Camsari[2] & Joerg Appenzeller[2,3]

Taking advantage of the magnetoelectric and its inverse effect, this article demonstrates strain-mediated magnetoelectric write and read operations simultaneously in $Co_{60}Fe_{20}B_{20}/Pb(Mg_{1/3}Nb_{2/3})_{0.7}Ti_{0.3}O_3$ heterostructures based on a pseudo-magnetization $\mu \equiv m_x^2 - m_y^2$. By applying an external DC-voltage across a (011)-cut PMN-PT substrate, the ferroelectric polarization is re-oriented, which results in an anisotropic in-plane strain that transfers to the CoFeB thin film and changes its magnetic anisotropy H_k. The change in H_k in-turn results in a 90° rotation of the magnetic easy axis for sufficiently high voltages. Simultaneously, the inverse effect is employed to read changes of the magnetic properties. The change of magnetization in ferromagnetic (FM) layer induces an elastic stress in the piezoelectric (PE) layer, which generates a PE potential that can be used to readout the magnetic state of the FM layer. The experimental results are in excellent qualitative agreement with an equivalent circuit model that considers how magnetic properties are electrically controlled in such a PE/FM heterostructure and how a back-voltage is generated due to changing magnetic properties in a self-consistent model. We demonstrated that a change of easy axis of magnetization due to an applied voltage can be directly used for information processing, which is essential for future ME based devices.

Recently, so-called Magnetoelectric (ME) effects[1–4] in piezoelectric (PE)/FerroMagnetic (FM) structures have attracted substantial research interest, since these may open a path towards controlling magnetic properties by means of an electric field—rather than currents—to achieve low energy dissipation in the writing process of magnetic memory cells[5–22]. As to the reading process, the Giant Magneto-Resistance (GMR)[18] or Tunneling Magneto-Resistance (TMR)[1] is usually utilized to readout the stored magnetic information. However, the readout energy based on magneto-resistive methods is not negligible compared with the extremely low writing energies. In addition, the integration of GMR or Magnetic Tunnel Junction (MTJ) stacks with piezoelectric substrates remains a challenge. This raises the question whether voltages that are used in case of the write operation could also be used in a reverse configuration to read the magnetic information in a more power efficient way. To demonstrate this idea, in this article, we have measured the reciprocal ME effect simultaneously and achieved a strain-mediated magnetoelectric write and read unit in a $Co_{60}Fe_{20}B_{20}/Pb(Mg_{1/3}Nb_{2/3})_{0.7}Ti_{0.3}O_3$ heterostructure based on a pseudo-magnetization $\mu \equiv m_x^2$-m_y^2 rather than a net magnetization m_x, m_y or m_z. Single crystal PMN-PT with (011) orientation was employed in this work as the piezoelectric substrate for achieving large ME effects due to its large piezoelectric coefficients with $d_{31} \sim -3{,}100$ pC/N along the [100] direction and $d_{32} \sim 1{,}400$ pC/N along the [01-1] direction[23–29].

The write operation in the magnetic subsystem is accomplished by applying an external DC-voltage across a (011)-cut PMN-PT substrate. The re-orientation of the ferroelectric polarization results in an anisotropic in-plane strain[16], which transfers to the CoFeB thin film and changes its H_k[1,16]. The change in H_k in-turn results in

[1]Department of Physics and Astronomy, Purdue University, West Lafayette, IN 47907, USA. [2]School of Electrical and Computer Engineering, Purdue University, West Lafayette, IN 47907, USA. [3]Birck Nanotechnology Center, Purdue University, West Lafayette, IN 47907, USA. [4]These authors contributed equally: Tingting Shen and Vaibhav Ostwal. ✉email: shen168@purdue.edu; vostwal@purdue.edu

	Bit 1	Bit 0
Spin-torque devices	$<m_x> = 1$	$<m_x> = -1$
Strain control devices	$\mu = <m_x^2 - m_y^2> = 1$	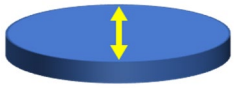 $\mu = <m_x^2 - m_y^2> = -1$

Table 1. Schematic diagram of bit states 0 and 1 in spin-torque devices and magnetoelectric(ME) devices represented by the red and yellow arrows respectively.

a 90° rotation of the magnetic easy axis for high enough voltages. On the other hand, to characterize the inverse effect, an AC magnetic field is simultaneously applied in the hard axis direction of the CoFeB film to induce an AC magnetization change. As a feedback, this AC magnetization change in CoFeB introduces strain in the substrate and generates a readout voltage across the PMN-PT[3,4]. Since the AC magnetization change is dependent on the H_k of the CoFeB which is being controlled by the DC voltage applied to the PMN-PT, the AC voltage generated (READ) across the PMN-PT is controlled by the external DC voltage applied (WRITE). Taking advantage of the coupling between the magnetic and electric effects, we have achieved both, electrical write and read operation in CoFeB/PMN-PT heterostructures by modulating the easy axis of the CoFeB film with a DC voltage and reading out this modulation through the detected AC voltage across the PMN-PT substrate. Compared with the work reported in Ref. 3, our measurement technique of the electrical read-out is completely different and is based on an AC excitation of the ferromagnetic film. Unlike Ref. 3, the electrical response from the substrate follows the AC drive of the magnetization at different DC-bias points, which indicates that in our experiment WRITE and READ operations are simultaneously demonstrated, in other words, the electrical voltage that is produced at the output (READ) is instantaneously following the magnetic field drive (WRITE) in our experiment. This is in stark contrast with Ref. 3 that shows WRITE and READ operations sequentially for memory applications.

The need for simultaneous READ and WRITE can be understood by considering potential devices that are not necessarily memory devices. For example, in a field effect transistor the change of channel resistance controlled by an applied gate voltage (WRITE) can be read-out by the source-drain current almost instantaneously. Similarly, it is possible to imagine magnetoelectric devices that generate an output voltage (READ) as a function of magnetization that is being driven by an external input, like a transistor. We discuss the possibility of such a device that can function as a tunable random number generator in Fig. 2c.

Our experimental results that are discussed below are in excellent qualitative agreement with a recently proposed equivalent circuit[4] that considers how the easy axis of an FM is changed due to an applied voltage and how a back-voltage (v_m) is generated in the PE due to this change in a self-consistent model. The key novelty of our work is to argue that a change of easy axis of magnetization due to an applied voltage can be directly used for information processing and suggests a different mode of operation from normal magnetic random-access memory (MRAM) technology. This difference is illustrated in Table 1, which shows schematically the bit states 0 and 1.

For nanomagnets with an easy axis in the x-direction, conventional current controlled spin-torque devices store the bit information in the form of a net magnetization i.e. $<m_x>$ or $<-m_x>$[23–25]. However, in voltage-controlled ME devices, although the energy dissipation is much lower than conventional current controlled spin-torque devices, a deterministic net magnetization flip is hard to achieve which hinders its practical applications. In this context, the change of easy axis of the nanomagnet under an applied voltage, which is defined as a pseudo-magnetization $\mu \equiv m_x^2 - m_y^2$ is proposed to be used in information processing[4]. In this paper, we have demonstrated that voltage-controlled pseudo-magnetization states can be written and read, which is an important step towards future spintronics devices.

Results and discussion

In this article, electrical detection of the pseudo-magnetization has been achieved in a $Co_{60}Fe_{20}B_{20}/Pb(Mg_{1/3}Nb_{2/3})_{0.7}Ti_{0.3}O_3$ heterostructure. Figure 1a shows the schematic configuration of the experimental set-up. The "sloppy" magnetic hysteresis loop measured along the [01-1] direction shown in Fig. 1b indicates the [01-1] direction is the hard axis of the CoFeB film, which is determined by a tensile strain in the [100] direction and a compressive strain in the [01-1] direction induced by the pre-poled (011)-cut PMN-PT substrate. Note that H_{DC} is pointing in the y-direction. The piezo-response of PMN-PT under an external DC voltage and the resulting modulation on the CoFeB magnetization properties are described in Figures S1 and S2 respectively. Figure 1c shows the pseudo-magnetization $\mu \equiv m_x^2 - m_y^2 = 1 - 2m_y^2$ as calculated from the MH loop in Fig. 1b.

To characterize the pseudo-magnetization information by electrical means in the PE/FM heterostructure, an AC magnetic field H_{AC} with an amplitude of 4Oe at a frequency of 112 Hz was applied in addition to a DC magnetic field in the [01-1] direction, which induces an AC magnetization change in the way shown by the yellow arrows in Fig. 1a. The change of magnetization induces deformation in the FM film due to the magnetostriction effect[30] which transmits to the PE substrate and results in a change of P due to the piezoelectric effect[31]. The

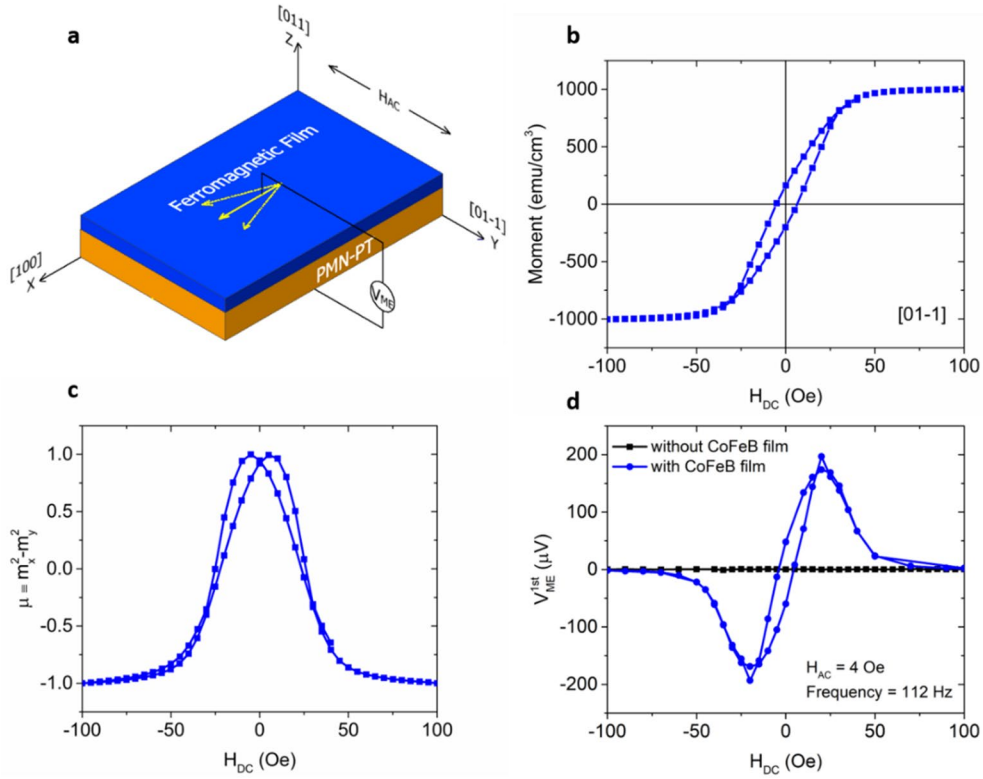

Figure 1. (**a**) Experimental set-up of detecting the pseudo-magnetization electrically. (**b**) Magnetic hysteresis loop of an Au(100 nm)/Ti(10 nm)/(011)-cut PMN-PT(300 μm)/CoFeB(40 nm)/Ta(5 nm) heterostructure measured along the [01-1] direction; (**c**) The corresponding pseudo-magnetization calculated by $\mu \equiv m_x^2 - m_y^2$. (**d**) The first harmonic magnetoelectric voltage measured across (011)-cut PMN-PT substrates with and without CoFeB film with an AC magnetic field applied in the [01-1] direction. The magnitude and frequency of the AC magnetic field is $H_{AC} = 4$Oe and f = 112 Hz respectively. The device structure for the black and blue curve is Au(100 nm)/Ti(10 nm)/(011)-cut PMN-PT(300 μm)/Ti(10 nm)/Au(100 nm) and Au(100 nm)/Ti(10 nm)/(011)-cut PMN-PT(300 μm)/CoFeB(40 nm)/Ta(5 nm) respectively.

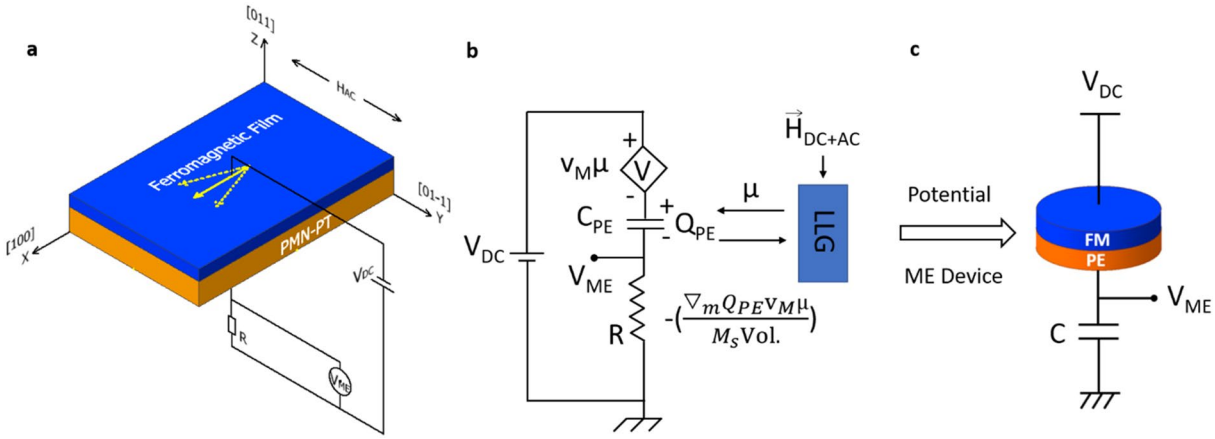

Figure 2. (**a**) Experimental set-up and (**b**) an equivalent circuit model for the PE/FM heterostructure that captures the simultaneous ME write and read operation based on the pseudo-magnetization proposed in Ref. 4. (**c**) A concrete ME device that could be used for practical applications, where the FM is fabricated as a low-barrier nanomagnet (see Ref. 4 for the detailed operation of the voltage-controlled ME device).

variation of P during the reorientation of the magnetization gives rise to a magnetoelectric voltage defined as V_{ME} across the heterostructure. The blue curve in Fig. 1d shows the first harmonic of the magnetoelectric voltage, i.e. V_{ME}^{1st} measured by a lock-in amplifier SR830. For an AC magnetic field of frequency 2π/w, the 1st and 2nd harmonic of V_{ME} is extracted using

$$V_{ME}^{1st} = \frac{1}{T}\int_0^T V_{ME}(t) * \sin(\mathrm{wt})\mathrm{dt} = \mathrm{H_{AC}} * \frac{\partial \mathrm{V_{ME}}}{\partial \mathrm{H_{DC}}} \tag{1}$$

$$V_{ME}^{2nd} = \frac{1}{T}\int_0^T V_{ME}(t) * \sin(2\mathrm{wt})\mathrm{dt} = (\mathrm{H_{AC}})^2 * \frac{\partial}{\partial \mathrm{H_{DC}}}\left(\frac{\partial \mathrm{V_{ME}}}{\partial \mathrm{H_{DC}}}\right) \tag{2}$$

where T = w/2π is the period of the AC magnetic field. According to the analysis in Ref. 3,4, $V_{ME} = v_m\mu$, where v_m is the back-voltage constant which will be discussed more later in the context of Fig. 2. Thus,

$$V_{ME}^{1st} = H_{AC} * \frac{\partial V_{ME}}{\partial H_{DC}} = H_{AC} * v_m * \frac{\partial \mu}{\partial H_{DC}} \tag{3}$$

$$V_{ME}^{2nd} = (H_{AC})^2 * \frac{\partial}{\partial H_{DC}}\left(\frac{\partial V_{ME}}{\partial H_{DC}}\right) = (H_{AC})^2 * v_m * \frac{\partial}{\partial H_{DC}}\left(\frac{\partial \mu}{\partial H_{DC}}\right) \tag{4}$$

Thus, the complicated shape of the detected V_{ME}^{1st} signal shown in the blue curve in Fig. 1d electrically characterizes the slope of $\mu(H_{DC})$ in Fig. 1c due to the AC magnetization change (V_{ME}^{2nd} will be discussed later in the context of Figure S3).

The black curve in Fig. 1d shows the first harmonic magnetoelectric voltage measured with a control sample, which consists of an identical (011)-cut PMN-PT substrate but with Ti (10 nm)/Au (100 nm) deposited on both top and bottom surfaces without a CoFeB film. In this case, we have observed no read-out signal which confirms that the magnetoelectric voltage measured across PMN-PT is induced by the CoFeB film.

Having established the principle of electrical read out of the pseudo-magnetization μ, we will discuss next the simultaneous ME write and read operation in the same PE/FM sample. (For a detailed discussion on the individual READ and WRITE process please see Supplementary Section II and III.) The experimental set-up is shown in Fig. 2a. Before moving on to the actual measurement results, we will discuss the measurement principle based on an equivalent circuit model illustrated in Fig. 2b[4]. This circuit has been experimentally benchmarked against the results reported in Ref. 3.

The magnetization dynamics of the FM layer are calculated from the Landau–Lifshitz–Gilbert equation self-consistently which takes the stress-induced anisotropy field through the charge on the PE capacitor as an input and produces the pseudo-magnetization $\mu \equiv m_x^2 - m_y^2$ as an instantaneous output. The circuit equation is given as:

$$V_{DC} = \frac{\partial E_M}{\partial Q_{PE}} + \frac{Q_{PE}}{C_{PE}} + R\frac{dQ_{PE}}{dt} \tag{5}$$

where E_M is the magnetic energy, C_{PE} is the capacitance of the PE material, Q_{PE} is the charge on the PE capacitor and R is a resistor connected in series with the PE/FM heterostructure. The write operation is accomplished by an effective field:

$$\vec{H}_{ME} = -\frac{\nabla_m E_M}{M_S Vol.} \tag{6}$$

where ∇_m is the gradient operator with respect to the magnetization directions m_i. M_S and Vol. are the saturation magnetization and the volume of the magnetic film respectively. The read operation is accomplished due to a changing "back-voltage" through the pseudo-magnetization μ, $V_{ME_tot} = \frac{\partial E_M}{\partial Q_{PE}} = v_m\mu$, and $E_M = Q_{PE}v_m\mu$.

To measure the magnetoelectric voltage using a lock-in amplifier, a resistor R with a resistance value comparable to the impedance of the piezoelectric capacitor is connected in series with the heterostructure. V_{ME}^{1st} and V_{ME}^{2nd} measured across R are used to read the magnetic information of the FM layer since they are proportional to the slope and curvature of $\mu(H_{DC})$ due to the AC magnetization change respectively as shown in Eqs. (3) and (4). MATLAB analytical simulations on simultaneous ME write and read operations are discussed in Figure S4.

In Fig. 2c, we illustrate the concept of a magntoelectric device that can be used for practical applications by employing a PE/FM stack in series with a capacitor, where the FM is fabricated as a low-barrier nanomagnet whose energy barrier is comparable to the thermal energy kT. If the magnet is fabricated as a circular magnet without any uniaxial anisotropy, the magnetization would fluctuate randomly in the plane due to the presence of thermal noise. Due to the back-voltage that would be induced by the fluctuations of magnetization, this 2-terminal device can operate as a voltage controllable tunable random number generator[32–37] that operates without any external magnetic fields[4].

Similar to the operation of this conceptual device, in our experiment the change in the magnetization of the FM is turned into changes in the output voltage, with the difference that instead of random fluctuations the magnetization is being deterministically driven by external magnetic fields. In practical applications involving low barrier magnets, such external DC or AC magnetic fields would not be required since magnetization would naturally be driven by thermal noise.

Experimentally, the PE/FM heterostructure used in this measurement is CoFeB (40 nm)/(011)-cut PMN-PT (300 μm) with Ta and Ti/Au as the top and bottom electrodes respectively. Voltage-controlled magnetization

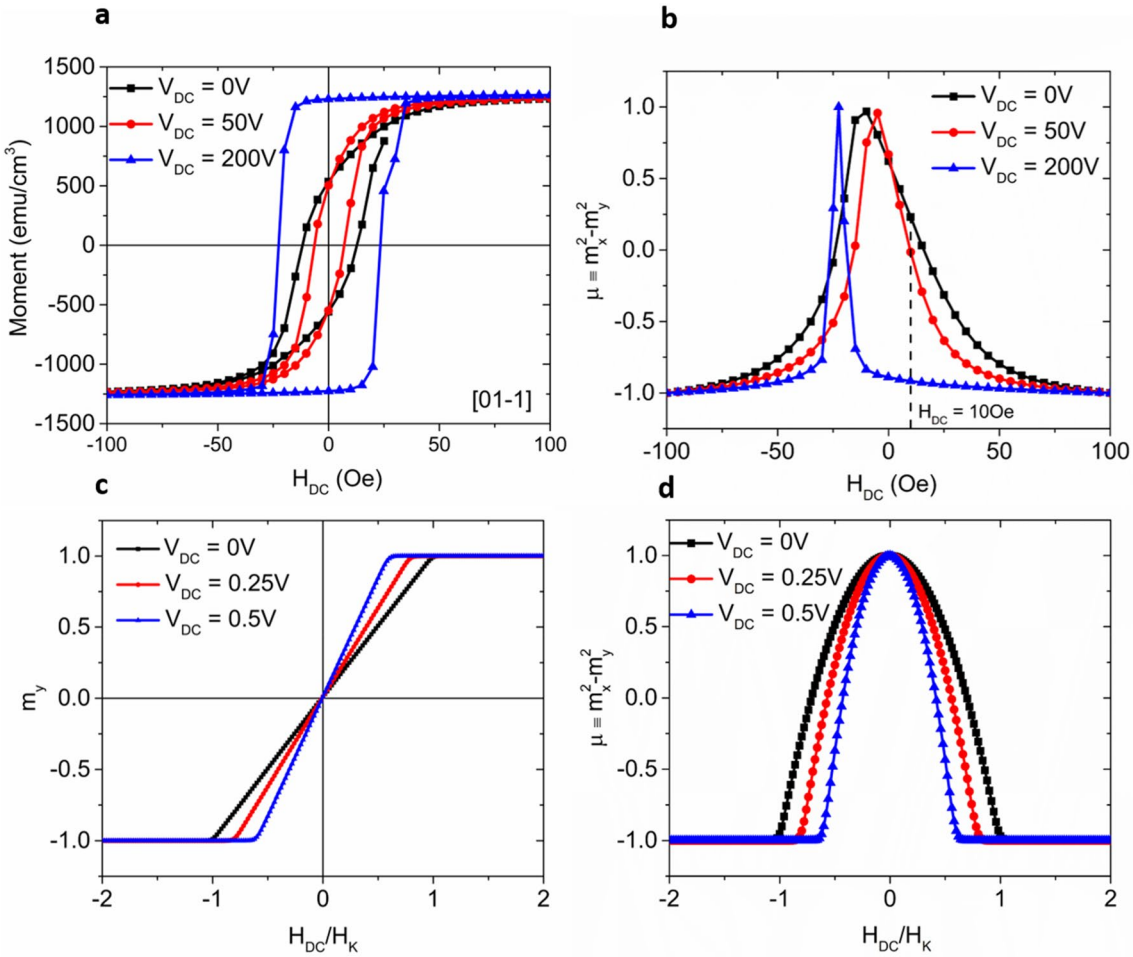

Figure 3. (**a**) M–H loops of an Au(100 nm)/Ti(10 nm)/(011)-cut PMN-PT(300 μm)/CoFeB(40 nm)/Ta(5 nm) heterostructure measured along the [01-1] direction under different voltages. (**b**) The corresponding pseudo-magnetization calculated from the data in (**a**) using $\mu \equiv m_x^2 - m_y^2$. (c) SPICE simulation results on the average in-plane hard axis magnetization m_y as a function of DC magnetic field in the y-direction at different DC voltages (V_{DC}). (**d**) The corresponding pseudo-magnetization calculated from $\mu \equiv m_x^2 - m_y^2$. Without loss of generality, the following parameters are used in the numerical circuit: $H_K = 25$ Oe, Ms = 300 emu/cc, Vol. = 5e−13 cm^3, damping coefficient $\alpha = 0.1$, demagnetization field H_D is assumed to be 100 H_K. The piezoelectric capacitance C_{PE} is chosen to be 7.5 pF, and the load resistance is 0.1 Ω.

measurements were carried out in a Magnetic Property Measurement System (MPMS) at room temperature. Figure 3a shows the stack's magnetic hysteresis loops measured along the [01-1] direction under different voltages. In all measurements, "positive DC voltage" means that the bottom electrode has a higher (more positive) potential than the top electrode. With DC voltages applied in the [011] crystalline direction, a strong in-plane anisotropic piezo-strain is induced due to the re-orientation of the ferroelectric polarization (P)[31,38–40] which transfers to the CoFeB thin film and provides an in-plane magnetic anisotropic field that changes the magnet's H_k. When the strain is sufficiently large, the result is a 90° rotation of the magnetic easy axis[1,16]. It is worth mentioning that an interfacial charge-mediated ME coupling effect may also induce magnetization modulations in the FM layer. However, the spatial extent of this interfacial modulation is typically less than 1–2 nm, which is too small to account for the large magnetization modulation observed in our experiment.

As discussed in Fig. S1, under large positive voltages [case 2 in Fig. S1], there is a tensile strain in the [01-1] direction and a compressive strain in the [100] direction, which favors a magnetization along the [01-1] direction and results in a high remnant magnetization as evident from Fig. 3a. Figure 3b shows the calculated pseudo-magnetization when scanning H_{DC} from 100Oe to − 100Oe. It is obvious that both the line width and the slope of $\mu(H_{DC})$ have been modulated by V_{DC}.

Furthermore, the experimental results are described qualitatively by theoretical simulations using the equivalent circuit shown in Fig. 2b. Figure 3c shows the average magnetization at different input voltages, verifying the easy-axis anisotropy modulation by different input voltages which qualitatively agrees with the experimental results in Fig. 3a. The corresponding pseudo-magnetization $\mu \equiv m_x^2 - m_y^2$ is shown in Fig. 3d.

Note that we have not attempted a quantitative benchmarking of the experiment, which is why the V_{DC} values in Fig. 3b, d are not the same. Another notable difference between the experiments and simulations is that we

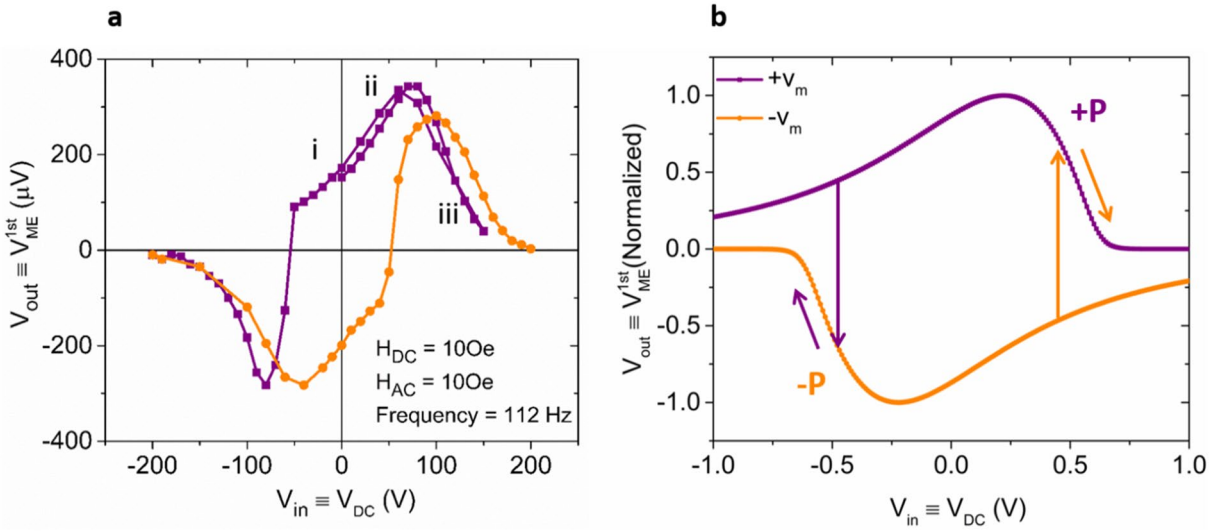

Figure 4. (**a**) Experimental results on the relation between $V_{in} \equiv V_{DC}$ and $V_{out} \equiv V_{ME}^{1st}$ when $H_{DC} = 10$Oe, $H_{AC} = 10$Oe and the frequency of the AC field is 112 Hz. The purple and orange lines represent scanning $V_{in} \equiv V_{DC}$ from + 200 to − 200 V and from − 200 to + 200 V respectively. (**b**) The purple and orange lines are simulation results on V_{ME}^{1st} as a function of V_{DC} at a fixed DC magnetic field corresponding to 0.5 H_{DC}/H_K that is read out from the circuit in Fig. 2b when the back-voltage constant is + v_m and − v_m respectively. Since our simulation does not capture a voltage controlled ferroelectric polarization switching, positive and negative v_m values had to be used in the simulation. The arrows indicate how V_{out} versus V_{in} would behave once polarization switching is considered. Note that for the normalized V_{ME}^{1st} the actual value of the back-voltage v_m does not change the simulation results.

assumed the magnetic layer behaves like a monodomain nanomagnet without hysteresis in the hard-axis M-H curves, which results in the same pseudo-magnetization peak positions under different voltages in Fig. 3d. The experiment involves an un-patterned CoFeB film whose magnetization dynamics are very likely dependent on multi-domain behavior. The external voltage modulated hysteresis causes a shift of the pseudo-magnetization peak positions in Fig. 3b. Moreover, in the simulations, we have chosen a much thinner dielectric with a smaller area to keep relatively low capacitances to allow transient, SPICE-level circuit simulations.

Simultaneous with the modulated pseudo-magnetization by the external DC voltage, the magnetoelectric voltage V_{ME} was measured using the experimental set-up shown in Fig. 2a. Experimental results on V_{ME}^{1st} measured across R with an AC magnetic field superimposed on a DC magnetic field along the [01-1] direction when $V_{DC} = 0$ V, 20 V and 50 V are shown in Figure S5. Figure S5(c) shows simulation results of the normalized in-phase component of the AC voltage V_{ME}^{1st} as a function of DC magnetic fields that is read out from the circuit in Fig. 2b.

When envisioning a device application, the idea is to use voltage-to-spin conversion for the write operation and spin-to-voltage conversion for the read. Thus, the types of device characteristics that are desirable would have a voltage input V_{in} and voltage output V_{out}, with the magnetic information mediating between the two. To show how an input DC voltage, can control indeed in our devices a V_{ME} output voltage, we have fixed H_{DC} at 10Oe and have swept V_{in} between − 200 and 200 V. As shown in Fig. 4a, b, the relationship between $V_{in} \equiv V_{DC}$ and $V_{out} \equiv V_{ME}^{1st}$ are non-monotonic in both experiment and SPICE-simulations. This is the case since the slope of $\mu(H_{DC})$ which represents the magnitude of V_{ME}^{1st} is different for different V_{DC}-values due to the change of H_k in the CoFeB film according to the explanation in Fig. 3. For example, in Fig. 3b, when H_{DC} is fixed at 10Oe, the slope of μ increases when V_{DC} increases from 0 to 50 V and then decreases when V_{DC} increases to 200 V. Thus, for the states (1) through (3) in Fig. 4a, one obtains a maximum in V_{ME}^{1st} for (2). The abrupt switch in both the purple and orange lines around + /− 50 V corresponds to the piezoelectric polarization (P) switching when scanning V_{DC}. The relation between the piezoelectric polarization P and V_{ME}^{1st} is shown in Fig. S6 indicating $V_{ME}^{1st}(P) = -V_{ME}^{1st}(-P)$.

Figure 4b illustrates simulation results on the normalized V_{ME}^{1st} as a function of V_{DC} at a fixed DC magnetic field corresponding to 0.5 H_{DC}/H_K that is read out from the circuit in Fig. 2b. Note that to capture the hysteretic nature of V_{ME}^{1st} versus V_{DC} in the simulation, the coefficient v_m is made negative when the polarization switched. Compared with Fig. 4a, all the experimental results are in good qualitative agreement with those predicted by the circuit model.

Next, to extract the back-voltage constant in our experimental heterostructure, we performed a quantitative benchmarking of our results. Experimentally, when $V_{in} = 50$ V, $V_{ME}^{1st} = 290$ μV with $H_{AC} = 10$Oe and $H_k = 70$Oe read from the M–H loop shown in Fig. 3a. SPICE simulations were performed after considering the circuit loss factor $\frac{|jwRC|}{|jwRC+1|} = 0.37$ in the experimental set-up and all other experimental parameters. The coefficient v_m was calculated to be 5.5 mV according to Eq. (1) and the analysis in the context of Fig. 2 to match the experimental value of $V_{ME}^{1st} = 290$ μV when $\frac{H_{AC}}{H_k} = \frac{10Oe}{70Oe}$. v_m is a measure of the particular coupling strength between the chosen PE and FM materials. Based on two assumptions that: (1) lossless and elastic strain transfer from the FM to the PE and (2) the thickness of PE layer being much larger than the FM thickness, a theoretical value v_m can be

calculated from $v_m = \frac{Bdt_{FM}}{2\varepsilon}$ using the thickness of the FM layer $t_{FM} = 40$ nm, the magneto-elastic constant $B = -4$MPa[41], the net PE constant $d = d_{31} - d_{32} = 4{,}500$ pm/V, and the permittivity of the PE layer $\varepsilon = 600\varepsilon_0$[4]. The estimated $v_m = 70$ mV is about one order of magnitude higher than the one extracted from the experimental results. As a point of reference, from the experimental results in Ref. 3 on [N*($TbCo_2$/FeCo)]/PMN-PT (N is the layer number) a v_m of 37 mV can be extracted according to the analysis in Ref. 4. Using $v_m = \frac{Bdt_{FM}}{2\varepsilon}$ on the other hand, one finds $v_m = 49$ mV for the experiment in Ref. 3. While in both cases the experimentally extracted v_m is lower than the calculated one, we believe that the larger discrepancy in our case is likely a result of the non-ideal interface coupling between CoFeB and PMN-PT layers which may be influenced by a variety of factors. For example, the Joule magnetostriction associated with domain movements in the FM layer plays an important role in determine the strength of interface coupling. Since the ME effects involves dynamic magneto-mechanical coupling, unimpeded domain-wall motion, domain rotation are key requirements for the FM layer. Thus, a soft, high initial permeability and high magnetostriction ferromagnetic layer is preferred for strong ME effects. Moreover, the interface quality between the PE and FM layers is also important. This is because defects, inhomogeneities, grain boundaries and growth-induced stress may pin the domain and limit wall motion and rotation. In summary, to achieve a high v_m in PE/FM heterostructures, a magnetic layer with favorable domain dynamics and an interface free of growth-induced stress or defects are desired in practical applications[42,43].

In conclusion, taking advantage of the coupling between magnetic and electric effects, we have achieved both, electrical write and read operation in CoFeB/PMN-PT heterostructures simultaneously based on a voltage tunable pseudo-magnetization where $V_{in} = 0$ V corresponds to state 1 (the case when the easy axis of the CoFeB film is in the x-direction) and $V_{in} = \pm 200$ V corresponds to the state 0 (the case when the easy axis of the CoFeB film is in the y-direction). Since the strain induced in the PMN-PT is proportional to the electrical field applied across the structure, a 30 nm film would allow decreasing the write voltage V_{in} to ± 20 mV, making our approach attractive for various magnetic device applications. Moreover, our experimental results are qualitatively consistent with the theoretical simulations of an equivalent circuit reported in Ref. 4. In this work, a novel magnetic operation mode is proposed where a pseudo-magnetization $\mu = m_x^2 - m_y^2$ rather than a net magnetization m_x, m_y or m_z is used as the bit states in MRAM technology. The experimental and theoretical work reported here promises the feasibility of magnetic field free magneto-electric read and write operations in a magnetic system by utilizing a PE/FM stack using a low-barrier nano-magnet to obtain an ultra-low power tunable random number generator[4], which is significant for the development of voltage-controlled spintronics and low power, high-speed data storage technology.

Methods

Fabrication. Amorphous CoFeB films were deposited on one side of the poled (011)-cut PMN-PT substrate in a multisource magnetron sputtering system with a base pressure of 3E-8 Torr. After this, a 5 nm Ta capping layer was deposited in the same chamber. On the other side of the PMN-PT substrate, a 10 nm Ti seeding layer was deposited in a e-beam evaporation system followed by a 100 nm Au film as a bottom electrode of the PE/FM heterostructure.

SPICE simulation. The equivalent circuit SPICE model calculates a time dependent magnetization and voltage, allowing us to replicate even dynamics of the experimental measurement self-consistently. The following parameters of the ferromagnetic layer were used in the numerical circuit: $H_K = 25$ Oe, Ms = 300 emu/cc, Vol. = 5e−13 cm^3, damping coefficient $\alpha = 0.1$, demagnetization field H_D is assumed to be 100 H_K. The piezoelectric capacitance C_{PE} is chosen to be 7.5 pF, and the load resistance is 0.1 Ω. To calculate the ME voltage, first a constant DC field is applied to the FM in the in-plane hard axis [01-1] direction during the entirety of the transient simulation (10 ns for the present case). After the first 5 ns to allow for the magnet dynamics to reach a steady state, an AC magnetic field with a 500 MHz frequency and amplitude of 0.1 H_K is applied along the same direction.

Received: 20 April 2020; Accepted: 10 June 2020
Published online: 01 July 2020

References

1. Li, P. *et al.* Electric field manipulation of magnetization rotation and tunneling magnetoresistance of magnetic tunnel junctions at room temperature. *Adv. Mater.* **26**, 4320–4325 (2014).
2. Khan, A., Nikonov, D. E., Manipatruni, S., Ghani, T. & Young, I. A. Voltage induced magnetostrictive switching of nanomagnets: strain assisted strain transfer torque random access memory. *Appl. Phys. Lett.* **104**, 262407 (2014).
3. Klimov, A. *et al.* Magnetoelectric write and read operations in a stress-mediated multiferroic memory cell. *Appl. Phys. Lett.* **110**, 222401 (2017).
4. Camsari, K. Y., Faria, R., Hassan, O., Sutton, B. M. & Datta, S. Equivalent circuit for magnetoelectric read and write operations. *Phys. Rev. Appl.* **9**, 044020 (2018).
5. Gopman, D. B. *et al.* Strain-assisted magnetization reversal in Co/Ni multilayers with perpendicular magnetic anisotropy. *Sci. Rep.* **6**, 27774 (2016).
6. Staruch, M. *et al.* Reversible strain control of magnetic anisotropy in magnetoelectric heterostructures at room temperature. *Sci. Rep.* **6**, 37429 (2016).
7. Liu, M. *et al.* Voltage tuning of ferromagnetic resonance with bistable magnetization switching in energy-efficient magnetoelectric composites. *Adv. Mater.* **25**, 1435–1439 (2013).
8. Liu, M. *et al.* Giant electric field tuning of magnetic properties in multiferroic ferrite/ferroelectric heterostructures. *Adv. Funct. Mater.* **19**, 1826–1831 (2009).
9. Heron, J. T. *et al.* Deterministic switching of ferromagnetism at room temperature using an electric field. *Nature* **516**, 370 (2014).

10. Miura, K. *et al.* Voltage-induced magnetization dynamics in CoFeB/MgO/CoFeB magnetic tunnel junctions. *Sci. Rep.* **7**, 42511 (2017).
11. Peng, B. *et al.* Deterministic switching of perpendicular magnetic anisotropy by voltage control of spin reorientation transition in $(Co/Pt)_3$/Pb $(Mg_{1/3}Nb_{2/3})O_3$–$PbTiO_3$ multiferroic heterostructures. *ACS Nano* **11**, 4337–4345 (2017).
12. Zhao, Z. *et al.* Giant voltage manipulation of MgO-based magnetic tunnel junctions via localized anisotropic strain: a potential pathway to ultra-energy-efficient memory technology. *Appl. Phys. Lett.* **109**, 092403 (2016).
13. Meng, H. *et al.* Electric field effects in low resistance CoFeB–MgO magnetic tunnel junctions with perpendicular anisotropy. *Appl. Phys. Lett.* **100**, 122405 (2012).
14. Wang, W. G., Li, M., Hageman, S. & Chien, C. L. Electric-field-assisted switching in magnetic tunnel junctions. *Nat. Mater.* **11**, 64 (2012).
15. Wang, Q. *et al.* Strain-mediated 180 switching in CoFeB and Terfenol-D nanodots with perpendicular magnetic anisotropy. *Appl. Phys. Lett.* **110**, 102903 (2017).
16. Zhang, S. *et al.* Giant electrical modulation of magnetization in $Co_{40}Fe_{40}B_{20}$/$Pb(Mg_{1/3}Nb_{2/3})_{0.7}Ti_{0.3}O_3$ (011) heterostructure. *Sci. Rep.* **4**, 3727 (2014).
17. Zhang, S. *et al.* Electric-field control of nonvolatile magnetization in $Co_{40}Fe_{40}B_{20}$/$Pb(Mg_{1/3}Nb_{2/3})_{0.7}Ti_{0.3}O_3$ structure at room temperature. *Phys. Rev. Lett.* **108**, 137203 (2012).
18. Liu, M. *et al.* Electric field modulation of magnetoresistance in multiferroic heterostructures for ultralow power electronics. *Appl. Phys. Lett.* **98**, 222509 (2011).
19. Fetisov, Y. K., Petrov, V. M. & Srinivasan, G. Inverse magnetoelectric effects in a ferromagnetic–piezoelectric layered structure. *J. Mater. Sci.* **22**, 2074–2080 (2007).
20. Biswas, A. K., Bandyopadhyay, S. & Atulasimha, J. Complete magnetization reversal in a magnetostrictive nanomagnet with voltage-generated stress: a reliable energy-efficient non-volatile magneto-elastic memory. *Appl. Phys. Lett.* **105**, 072408 (2014).
21. Xiong, R. *et al.* Electric-field tuning of ferromagnetic resonance in CoFeB/MgO magnetic tunnel junction on a piezoelectric PMN-PT substrate. *Appl. Phys. Lett.* **111**, 062401 (2017).
22. Chen, A. *et al.* Giant nonvolatile manipulation of magnetoresistance in magnetic tunnel junctions by electric fields via magnetoelectric coupling. *Nat. Commun.* **10**, 243 (2019).
23. Liu, L. *et al.* Spin-torque switching with the giant spin Hall effect of tantalum. *Science* **336**, 555–558 (2012).
24. Locatelli, N., Cros, V. & Grollier, J. Spin-torque building blocks. *Nat. Mater.* **13**, 11 (2014).
25. Liu, L., Lee, O. J., Gudmundsen, T. J., Ralph, D. C. & Buhrman, R. A. Current-induced switching of perpendicularly magnetized magnetic layers using spin torque from the spin Hall effect. *Phys. Rev. Lett.* **109**, 096602 (2012).
26. Lai, Z. *et al.* Electric field-tailored giant transformation of magnetic anisotropy and interfacial spin coupling in epitaxial γ′-Fe_4N/$Pb(Mg_{1/3}Nb_{2/3})_{0.7}Ti_{0.3}O_3$(011) multiferroic heterostructures. *J. Mater. Chem. C.* **2019**(7), 8537–8545 (2019).
27. Li, Z., Mi, W. & Bai, H. Perpendicular magnetic anisotropy modulated by interfacial magnetoelectric coupling in Fe_4N/0.75$Pb(Mg_{1/3}Nb_{2/3})O_3$–$_{0.25}PbTiO_3$ multiferroic heterostructures. *J. Phys. D Appl. Phys.* **52**, 335001 (2019).
28. Lai, Z., Li, P. & Mi, W. Magnetoelectric coupling in γ′-Fe_4N/$Pb(Mg_{1/3}Nb_{2/3})_{0.7}Ti_{0.3}O_3$ multiferroic heterostructures. *J. Appl. Phys.* **2019**(126), 113901 (2019).
29. Liu, Y. *et al.* Electric-field control of magnetism in $Co_{40}Fe_{40}B_{20}$/(1–x)$Pb(Mg_{1/3}Nb_{2/3})O_{3-x}PbTiO_3$ multiferroic heterostructures with different ferroelectric phases. *ACS Appl. Mater. Interfaces* **2016**(8), 3784–3791 (2016).
30. Wang, D., Nordman, C., Qian, Z., Daughton, J. M. & Myers, J. Magnetostriction effect of amorphous CoFeB thin films and application in spin-dependent tunnel junctions. *J. Appl. Phys.* **97**, 10C906 (2005).
31. Park, S. E. & Shrout, T. R. Ultrahigh strain and piezoelectric behavior in relaxor based ferroelectric single crystals. *J. Appl. Phys.* **82**, 1804–1811 (1997).
32. Behin-Aein, B., Diep, V. & Datta, S. A building block for hardware belief networks. *Sci. Rep.* **6**, 29893 (2016).
33. Faria, R., Camsari, K. Y. & Datta, S. Low-barrier nanomagnets as p-bits for spin logic. *IEEE Magn. Lett.* **8**, 1–5 (2017).
34. Camsari, K. Y., Faria, R., Sutton, B. M. & Datta, S. Stochastic p-bits for invertible logic. *Phys. Rev. X* **7**, 031014 (2017).
35. Sutton, B., Camsari, K. Y., Behin-Aein, B. & Datta, S. Intrinsic optimization using stochastic nanomagnets. *Sci. Rep.* **7**, 44370 (2017).
36. Pervaiz, A. Z., Ghantasala, L. A., Camsari, K. Y. & Datta, S. Hardware emulation of stochastic p-bits for invertible logic. *Sci. Rep.* **7**, 10994 (2017).
37. Camsari, K. Y., Faria, R., Hassan, O., Pervaiz, A. Z., Sutton, B. M. & Datta, S. p-transistors and p-circuits for Boolean and non-Boolean logic. In *Spintronics X*, Vol. 10357, 103572K (International Society for Optics and Photonics, 2017).
38. Peng, J. *et al.* Orientation dependence of transverse piezoelectric properties of 0.70$Pb(Mg_{1/3}Nb_{2/3})O_3$–0.30$PbTiO_3$ single crystals. *Appl. Phys. Lett.* **85**, 6221–6223 (2004).
39. Li, F. *et al.* Composition and phase dependence of the intrinsic and extrinsic piezoelectric activity of domain engineered (1–x) $Pb(Mg_{1/3}Nb_{2/3})O_3$–x $PbTiO_3$ crystals. *J. Appl. Phys.* **108**, 034106 (2010).
40. Sun, E., Zhang, S., Luo, J., Shrout, T. R. & Cao, W. Elastic, dielectric, and piezoelectric constants of Pb $(In_{1/2}Nb_{1/2})O_3$–$Pb(Mg_{1/3}Nb_{2/3})O_3$–$PbTiO_3$ single crystal poled along [011] c. *Appl. Phys. Lett.* **97**, 032902 (2010).
41. Gowtham, P. G., Stiehl, G. M., Ralph, D. C. & Buhrman, R. A. Thickness-dependent magnetoelasticity and its effects on perpendicular magnetic anisotropy in Ta/CoFeB/MgO thin films. *Phys. Rev. B* **93**, 024404 (2016).
42. Srinivasan, G. *et al.* Magnetoelectric bilayer and multilayer structures of magnetostrictive and piezoelectric oxides. *Phys. Rev. B* **64**, 214408 (2001).
43. Srinivasan, G., Rasmussen, E. T. & Hayes, R. Magnetoelectric effects in ferrite-lead zirconate titanate layered composites: the influence of zinc substitution in ferrites. *Phys. Rev. B* **2003**(67), 014418 (2003).

Acknowledgements

This work was supported in part by the Center for Probabilistic Spin Logic for Low-Energy Boolean and Non-Boolean Computing (CAPSL), one of the Nanoelectronic Computing Research (nCORE) Centers as task 2759.003 and 2759.004, a Semiconductor Research Corporation (SRC) program sponsored by the NSF through CCF 1739635. The authors thank the staff at the Birck Nanotechnology center for their technical support. T. Shen is thankful for the help from Neil Dilley for discussions about experimental measurements.

Author contributions

T.S. worked on the device fabrication, characterization and data analysis; V.O. worked on characterization, data analysis and MATLAB analytical simulation. K.Y.C. worked on data analysis and HSPICE simulation of the circuit model. J.A. analyzed the data and oversaw the planning and execution of the project; T.S. wrote the manuscript.

Competing interests

The authors declare no competing interest.

Additional information

Supplementary information is available for this paper at https://doi.org/10.1038/s41598-020-67776-y.

Correspondence and requests for materials should be addressed to T.S. or V.O.

Reprints and permissions information is available at www.nature.com/reprints.

Publisher's note Springer Nature remains neutral with regard to jurisdictional claims in published maps and institutional affiliations.

Open Access This article is licensed under a Creative Commons Attribution 4.0 International License, which permits use, sharing, adaptation, distribution and reproduction in any medium or format, as long as you give appropriate credit to the original author(s) and the source, provide a link to the Creative Commons license, and indicate if changes were made. The images or other third party material in this article are included in the article's Creative Commons license, unless indicated otherwise in a credit line to the material. If material is not included in the article's Creative Commons license and your intended use is not permitted by statutory regulation or exceeds the permitted use, you will need to obtain permission directly from the copyright holder. To view a copy of this license, visit http://creativecommons.org/licenses/by/4.0/.

© The Author(s) 2020